ARMY RESEARCH LABORATORY

Heuristic-Based Nuisance Parameter Estimation of Low-Cost Accelerometers for Guided Spin-Stabilized Projectiles

by Luisa D. Fairfax, James M. Maley, and Frank E. Fresconi

ARL-TR-6750 **December 2013**

NOTICES

Disclaimers

The findings in this report are not to be construed as an official Department of the Army position unless so designated by other authorized documents.

Citation of manufacturer's or trade names does not constitute an official endorsement or approval of the use thereof.

Destroy this report when it is no longer needed. Do not return it to the originator.

Army Research Laboratory
Aberdeen Proving Ground, MD 21005-5066

ARL-TR-6750 **December 2013**

Heuristic-Based Nuisance Parameter Estimation of Low-Cost Accelerometers for Guided Spin-Stabilized Projectiles

Luisa D. Fairfax, James M. Maley, and Frank E. Fresconi
Weapons and Materials Research Directorate, ARL

REPORT DOCUMENTATION PAGE	Form Approved OMB No. 0704-0188

1. REPORT DATE *(DD-MM-YYYY)*	2. REPORT TYPE	3. DATES COVERED (From - To)
December 2013	Final	January 2012–August 2013

4. TITLE AND SUBTITLE
Heuristic-Based Nuisance Parameter Estimation of Low-Cost Accelerometers for Guided Spin-Stabilized Projectiles

5a. CONTRACT NUMBER

5b. GRANT NUMBER

5c. PROGRAM ELEMENT NUMBER

6. AUTHOR(S)
Luisa D. Fairfax, James M. Maley, and Frank E. Fresconi

5d. PROJECT NUMBER
AH43

5e. TASK NUMBER

5f. WORK UNIT NUMBER

7. PERFORMING ORGANIZATION NAME(S) AND ADDRESS(ES)
U.S. Army Research Laboratory
ATTN: RDRL-WML-E
Aberdeen Proving Ground, MD 21005-5066

8. PERFORMING ORGANIZATION REPORT N6750UMBER
ARL-TR-6750

9. SPONSORING/MONITORING AGENCY NAME(S) AND ADDRESS(ES)

10. SPONSOR/MONITOR'S ACRONYM(S)

11. SPONSOR/MONITOR'S REPORT NUMBER(S)

12. DISTRIBUTION/AVAILABILITY STATEMENT
Approved for public release; distribution is unlimited.

13. SUPPLEMENTARY NOTES

14. ABSTRACT
Accelerometer measurement errors due to low-cost devices and minimal ground calibration significantly affect inertial navigation performance in a spin-stabilized projectile application. A method of compensating for these nuisance parameters is proposed that leverages the spin-stabilized projectile flight dynamics and sensor modeling in an extended Kalman filter. Nonlinear modeling and practical simplification of the in-flight measurements was undertaken. An estimator algorithm was designed and validated in simulation. Results illustrate the manner in which corrupted measurements are enhanced. Monte Carlo analysis suggests that the nuisance parameter estimation improves navigation accuracy by three orders of magnitude, and under certain conditions is sufficient to increase overall system precision over the ballistic performance for munitions in a global positioning system-denied environment.

15. SUBJECT TERMS
navigation, guided projectile, spin stabilization, accelerometers, affordable

16. SECURITY CLASSIFICATION OF:			17. LIMITATION OF ABSTRACT	18. NUMBER OF PAGES	19a. NAME OF RESPONSIBLE PERSON
a. REPORT	b. ABSTRACT	c. THIS PAGE			Luisa Fairfax
Unclassified	Unclassified	Unclassified	UU	28	19b. TELEPHONE NUMBER (*Include area code*) 410-306-0794

Standard Form 298 (Rev. 8/98)
Prescribed by ANSI Std. Z39.18

Contents

List of Figures

List of Tables

Acknowledgments

The authors gratefully acknowledge the sponsorship of the Project Manager for Combat Ammunition Systems and the technical contributions (including providing the flight system simulation) of the U.S. Army Armament Research, Development, and Engineering Center.

INTENTIONALLY LEFT BLANK.

1. Introduction

The motivation for this report is navigating low-cost guided projectiles. Recently, the global positioning system (GPS) has been successfully integrated into gun-launched munitions (*1–6*). GPS components may be a significant portion of the overall system cost. Furthermore, GPS technology requires an infrastructure that adds to the burden on an already uncertain battlefield. Terrain masking and active threats also influence the tactical operation of GPS navigation for precision munitions. Thus, GPS-denied navigation technologies are of great military interest.

Technologies for guiding fin-stabilized (*1, 4, 5, 7, 8*) and spin-stabilized (*6, 9, 10–12*) projectiles from a gun-launched platform are available in the literature. Feedback measurements required for guidance are often difficult to collect in the gun-launched environment. Sensors must survive the gun launch event (*13–17*). Additionally, gun launch may alter the basic functionality of sensor devices, which obfuscates ground calibration. Spin-stabilized projectiles rotate hundreds or thousands of times per second, which severely stresses the dynamic range and integration of sensors such as accelerometers and gyroscopes. Affordability is a major concern for any military application. Micro-electromechanical (MEM) accelerometers are relatively inexpensive but often feature higher noise characteristics than alternate accelerometer technologies. Unduly high labor cost is sometimes required to calibrate these measurement technologies into the final integrated flight vehicle.

This report overcomes some of these technical challenges for using accelerometers to navigate precision munitions. In-flight nuisance parameter estimation (*18–21*) is used to compensate for low-cost accelerometer measurement errors in the ballistic environment. A comprehensive body of work in launch and flight sciences (*22–26*) may be applied to underpin measurement modeling and estimation algorithms. High-fidelity flight modeling has been used in the past for aircraft (*27*) and fin-stabilized projectile (*28*) navigation. The goal of this work is simple accelerometer nuisance parameter estimation algorithms to enable inertial navigation of spin-stabilized projectiles with low-cost devices.

This report presents the nonlinear model of in-flight accelerometer measurements. Next, practical simplifications to the in-flight measurement model for guided spin-stabilized projectiles with limited control authority are outlined. Nuisance parameter estimation algorithms are developed and inertial navigation is reviewed. Monte Carlo launch and flight simulation results of a guided spin-stabilized projectile are described.

2. In-Flight Measurement Modeling

Accelerometers mounted in a projectile in atmospheric flight measure the specific aerodynamic force in the body frame. The aerodynamic forces encountered during flight depend on the atmosphere (e.g., density, wind) and flow around the projectile (e.g., Mach number, angle of attack). An expression for ideal accelerometer measurements located at an arbitrary point in the projectile body follows (*29*).

$$\vec{a}_M^B = \frac{1}{m}\vec{F}_A + \vec{\dot{\omega}}_{B/I} \times \vec{r}_{CG\to M} + \vec{\omega}_{B/I} \times \vec{\omega}_{B/I} \times \vec{r}_{CG\to M} \tag{1}$$

Ideal accelerometer signals are corrupted in practical transduction devices by errors in scale factor, misalignment, cross axis sensitivity, misplacement, bias, and noise. Modeling these terms provides the following relationship for the specific force at the center of gravity (CG) measured by a real-world accelerometer.

$$\begin{aligned}\vec{a}_{CG}^B = \vec{S}_M \vec{T}_{MB} \Big[\frac{1}{m}\vec{F}_A + \vec{\dot{\omega}}_{B/I} \times \left(\vec{r}_{CG\to M} + \vec{\varepsilon}_{r_{CG\to M}}\right) + \vec{\omega}_{B/I} \times \vec{\omega}_{B/I} \\ \times \left(\vec{r}_{CG\to M} + \vec{\varepsilon}_{r_{CG\to M}}\right) + \vec{\varepsilon}_B + \vec{\varepsilon}_N\Big]\end{aligned} \tag{2}$$

MEM accelerometers offer enormous advantages in terms of device size, gun-launched survivability, and cost due to economies of scale. These devices are improving performance drastically but still often fall short of guided-projectile requirements for inertial navigation.

After neglecting scale factor, misalignment, and nonorthogonality errors, an expression for the error in the accelerometer measurement at the CG may be obtained through a simple difference:

$$\vec{e}_{\vec{a}_{CG}^B} = \vec{\dot{\omega}}_{B/I} \times \vec{\varepsilon}_{r_{CG\to M}} + \vec{\omega}_{B/I} \times \vec{\omega}_{B/I} \times \vec{\varepsilon}_{r_{CG\to M}} + \vec{\varepsilon}_B + \vec{\varepsilon}_N \tag{3}$$

The measurement error in equation 3 can be manipulated for the spin-stabilized projectile application. Gyroscopic action is used to stabilize statically unstable projectiles. High projectile spin rates are necessary for achieving gyroscopic stability. Therefore, the spin rate is much higher than pitch and yaw rates ($p \gg q, r$) and dominates the centripetal acceleration term in equation 3. In contrast, the spin rate deceleration is very small compared with the other components of angular acceleration. However, the radial components are perfectly periodic with roll rate, and therefore have no net effect on accelerometer integration, so the tangential acceleration term is neglected. Using these assumptions, the equation for the error in the accelerometer measurement at the CG may be simplified to the following form.

$$e_{\vec{a}_{CG}^B} = cp^2 + b \tag{4}$$

This equation lumps some individual error parameters (e.g., scale factor, misalignment, bias) together into two separate terms, and uses an estimate of spin rate to model critical features of accelerometer errors for spin-stabilized projectiles.

Spin-stabilized flight dynamics may also be leveraged in modeling lateral accelerometers. Figure 1 provides the body-fixed coordinate system. Triaxial accelerometers are often mounted orthogonally with the principal axis of one accelerometer along the spin axis of the projectile (axial accelerometer), and the principal axes of the other two accelerometers are oriented to complete a right-hand coordinate system (lateral accelerometers). For right-hand-spun projectiles, the lateral accelerometer signals resemble sine waves with the J-axis measurement lagging the K-axis measurement by 90°. Over one revolution of spin the lateral accelerations have zero mean during the ballistic portion of flight. Lateral accelerometers were modeled with a parameter for the amplitude and using the appropriate sine/cosine function of spin rate since spin rate does not change appreciably over a revolution.

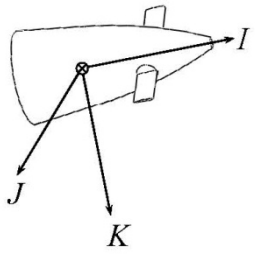

Figure 1. Body-fixed coordinate system.

Axial acceleration is driven by drag. Flight mechanics (*22, 23, 26*) and high-fidelity aerodynamic characterization (*25*) can be applied to estimate the specific axial force to within yaw-dependent axial force (usually small), manufacturing tolerances (e.g., mass, drag coefficient), and atmospheric uncertainties (e.g., density, wind) when velocity is obtained in flight.

$$a_i = -\frac{\pi}{8m}\rho D^2 C_X V^2 \tag{5}$$

This expression provides a heuristic-based calculation for using in the nuisance parameter estimation of the axial accelerometer.

3. Estimator Design

To perform the nuisance parameter estimation, an extended Kalman filter was created (*30*). The accelerometer model development for the spin-stabilized projectile environment outlined previously was incorporated into the estimator design. The state vector for the nuisance parameters are therefore the lateral accelerations, constant biases, and biases related to the roll rate squared, as shown:

$$\vec{X} = \begin{Bmatrix} a_j \sin(pt) \\ a_k \cos(pt) \\ b_i \\ b_j \\ b_k \\ (cp^2)_i \\ (cp^2)_j \\ (cp^2)_k \end{Bmatrix} \tag{6}$$

The measurements are the triaxial accelerometers.

$$\vec{Y} = \vec{a}_{CG}^{B} \tag{7}$$

The nuisance parameter state propagation equations are as follows:

$$\dot{\vec{X}} = \vec{A}\vec{X} \tag{8}$$

$$\vec{A} = \begin{bmatrix} 0 & p & 0 & 0 & 0 & 0 & 0 & 0 \\ -p & 0 & 0 & 0 & 0 & 0 & 0 & 0 \\ 0 & 0 & 0 & 0 & 0 & 0 & 0 & 0 \\ 0 & 0 & 0 & 0 & 0 & 0 & 0 & 0 \\ 0 & 0 & 0 & 0 & 0 & 0 & 0 & 0 \\ 0 & 0 & 0 & 0 & 0 & \left(\frac{2}{p}\dot{p}\right) & 0 & 0 \\ 0 & 0 & 0 & 0 & 0 & 0 & \left(\frac{2}{p}\dot{p}\right) & 0 \\ 0 & 0 & 0 & 0 & 0 & 0 & 0 & \left(\frac{2}{p}\dot{p}\right) \end{bmatrix} \tag{9}$$

Projectile roll dynamics (*22–24*, *26*) may be applied to obtain spin acceleration ($\dot{p} = \frac{\pi\rho VD^4 C_{l_p} p}{16}$). In discrete time, the state propagation matrix is

$$\vec{F} = e^{\bar{A}\Delta t} \tag{10}$$

$$\vec{F} \approx \begin{bmatrix} \cos(p\Delta t) & \sin(p\Delta t) & 0 & 0 & 0 & 0 & 0 & 0 \\ -\sin(p\Delta t) & \cos(p\Delta t) & 0 & 0 & 0 & 0 & 0 & 0 \\ 0 & 0 & 1 & 0 & 0 & 0 & 0 & 0 \\ 0 & 0 & 0 & 1 & 0 & 0 & 0 & 0 \\ 0 & 0 & 0 & 0 & 1 & 0 & 0 & 0 \\ 0 & 0 & 0 & 0 & 0 & 1+\frac{2\dot{p}}{p}\Delta t & 0 & 0 \\ 0 & 0 & 0 & 0 & 0 & 0 & 1+\frac{2\dot{p}}{p}\Delta t & 0 \\ 0 & 0 & 0 & 0 & 0 & 0 & 0 & 1+\frac{2\dot{p}}{p}\Delta t \end{bmatrix} \tag{11}$$

Between measurement updates, the state and covariance are propagated according to the following expressions.

$$X_k^- = F_{k-1} X_{k-1}^+ \tag{12}$$

$$P_k^- = F_{k-1} P_{k-1}^+ F_{k-1}^T + Q_{k-1} \tag{13}$$

A simplified model of the accelerometers is proposed based on modeling of the aforementioned in-flight measurements.

$$\vec{Y}^* = \begin{bmatrix} a_i + b_i + (cp^2)_i \\ a_j \sin(pt) + b_j + (cp^2)_j \\ a_k \cos(pt) + b_k + (cp^2)_k \end{bmatrix} \tag{14}$$

The relationship between the measurement model and the nuisance parameter states can be obtained from a partial derivative.

$$\vec{H} = \begin{bmatrix} \left(\frac{\partial \vec{Y}^*}{\partial(a_j \sin(pt))}\right) & \left(\frac{\partial \vec{Y}^*}{\partial(a_k \cos(pt))}\right) & \left(\frac{\partial \vec{Y}^*}{\partial b_i}\right) & \left(\frac{\partial \vec{Y}^*}{\partial b_j}\right) & \left(\frac{\partial \vec{Y}^*}{\partial b_k}\right) & \left(\frac{\partial \vec{Y}^*}{\partial (cp)_i}\right) & \left(\frac{\partial \vec{Y}^*}{\partial (cp)_j}\right) & \left(\frac{\partial \vec{Y}^*}{\partial (cp)_k}\right) \end{bmatrix} \tag{15}$$

And the resulting measurement matrix is

$$\vec{H} = \begin{bmatrix} 0 & 0 & 1 & 0 & 0 & 1 & 0 & 0 \\ 1 & 0 & 0 & 1 & 0 & 0 & 1 & 0 \\ 0 & 1 & 0 & 0 & 1 & 0 & 0 & 1 \end{bmatrix} \tag{16}$$

The Kalman gain, state, and covariance, respectively, are updated at each measurement.

$$\vec{K}_k = \vec{P}_k^- \vec{H} (\vec{H} \vec{P}_k^- \vec{H} + \vec{R})^{-1} \tag{17}$$

$$\vec{X}_k^+ = \vec{X}_k^- + \vec{K}_k \left[\vec{Y} - \left(\vec{H} \vec{X}_k^- + \begin{bmatrix} a_i \\ 0 \\ 0 \end{bmatrix} \right) \right] \tag{18}$$

$$\vec{P}_k^+ = (\vec{I} - \vec{K}_k \vec{H}) \vec{P}_k^- \tag{19}$$

Finally, the accelerometer measurement is compensated using these nuisance parameters.

$$\hat{a}_{CG}^B = \vec{Y} - \vec{Y}^* \tag{20}$$

The body acceleration of the CG is transformed into the inertial frame and the force of gravity is added for inertial navigation.

$$\vec{a}_{CG}^I = \vec{T}_{BI} \hat{a}_{CG}^B + \vec{\mathrm{g}} \tag{21}$$

A trapezoidal numerical integration scheme is applied to obtain inertial velocity and position from this acceleration. Initial velocity and position are necessary.

4. Simulation Setup

To validate the algorithm presented in the previous section, a guided artillery projectile equipped with a GPS, course-correcting fuze, and triaxial accelerometers was simulated in a Matlab/Simulink environment. The simulation features high-fidelity nonlinear models of flight (*11*), sensors, and actuators. The projectile was nominally launched at a 45° quadrant elevation and about 800 m/s, which resulted in flying over 20 km downrange. In the following studies, the projectile uses GPS navigation for guidance feedback, whereas the present algorithm is run in parallel solely to assess the effectiveness of the nuisance parameter estimation and corresponding navigation performance. All results for the inertial navigation use perfect initialization, attitude information, mass properties, aerodynamics, and atmosphere.

The nominal error budget for the accelerometers is shown in table 1. Note that the I-axis accelerometer can have a much smaller noise value because a part with a lower full-scale dynamic range, and thus higher sensitivity can be used since misposition errors are much less likely to result in clipping than with the J/K-axis sensors.

Table 1. Accelerometer error budget.

Description	Symbol	Value (1σ)
Scale-factor error	$\vec{S}_M$ (diagonals)	1% full-scale value
Nonorthogonality error	$\vec{S}_M$ (off-diagonals)	0.5% full-scale value
Misalignment error	$\vec{T}_{MB}$	0.5°
Turn-on bias error	$\varepsilon_{B,T}$	100 mG
Drift bias error	$\varepsilon_{B,D}$	4 mG
I-axis accelerometer noise	ε_{N_I}	4 mG
J/K-axis accelerometer	$\varepsilon_{N_{J/K}}$	150 mG
Nominal position	$\vec{r}_{CG\to M}$	$\{0.5 \quad 0 \quad 0\}^T$ m
Misplacement error	$\vec{\varepsilon}_{r_{CG\to M}}$	0.5 mm

5. Results

The simulation environment and algorithm implementation was first validated by turning all of the measurement errors to zero and assessing the integration errors due to computation. The launch conditions were randomly varied so that the projectile maneuvered differently to reach the target. To evaluate the performance of the algorithm, the root-sum-square (RSS) of the error between the position obtained from inertial measuring unit integration and the true position as a function of time will be used as a measurement of performance. The RSS position error at the time of impact provides the “miss distance” of the navigation, and the median of all miss distances provides an estimate of the navigation circular error probable (CEP), which will be used as a metric in the subsequent Monte Carlo experiments. A set of 100 computational error histories shown in figure 2 displays reasonable performance and validates the accelerometer modeling and algorithm implementation.

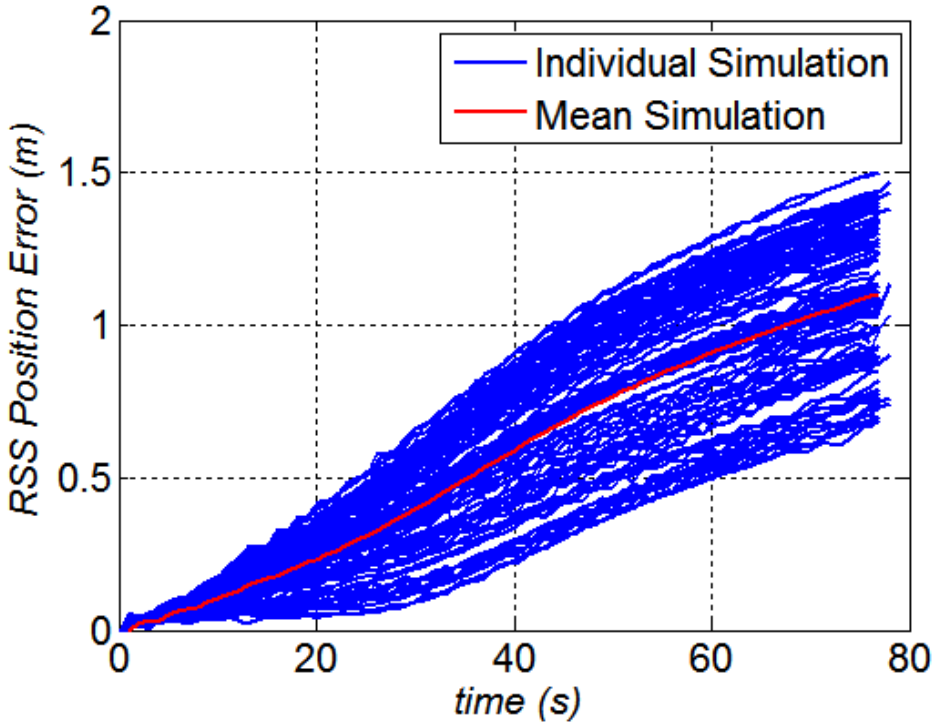

Figure 2. RSS position error due to computation with no sensor errors.

Even if the nuisance parameter estimation works flawlessly, the accuracy of the inertial navigation solution is limited by the random errors due to accelerometer noise and bias drift since these errors cannot be compensated for. To determine a lower bound for the inertial navigation, a set of 100 Monte Carlo flights were simulated with only the random noise and bias drift of the accelerometers active. The scalar position variance is described by the following function of time and integration sample time (*31*):*

$$\sigma_{err}^2(t) = \sigma_{noise}^2 \Delta t \frac{t^3}{5} + \sigma_{drift}^2 \Delta t \frac{t^5}{20} \tag{22}$$

The integration and algorithms were both run at a rate of 1 kHz. The highest frequency component of the radial accelerometer signals corresponds to the maximum spin rate, so the Nyquist frequency is just over 500 Hz. This must be balanced with realistic real-time processing limitations of embedded hardware. The rate of 1 kHz is feasible on an embedded processor, while providing some protection against aliasing. The results of the Monte Carlo analysis demonstrate that the measured variance is close to the theoretical variance (assuming the J/K-axis noise dominates), with a resultant navigation CEP of about 26 m at impact, demonstrated in figure 3.

* Even though the variance is a function of sample time, as the sample time approaches zero this approximation becomes invalid because the real-world white noise is band-limited.

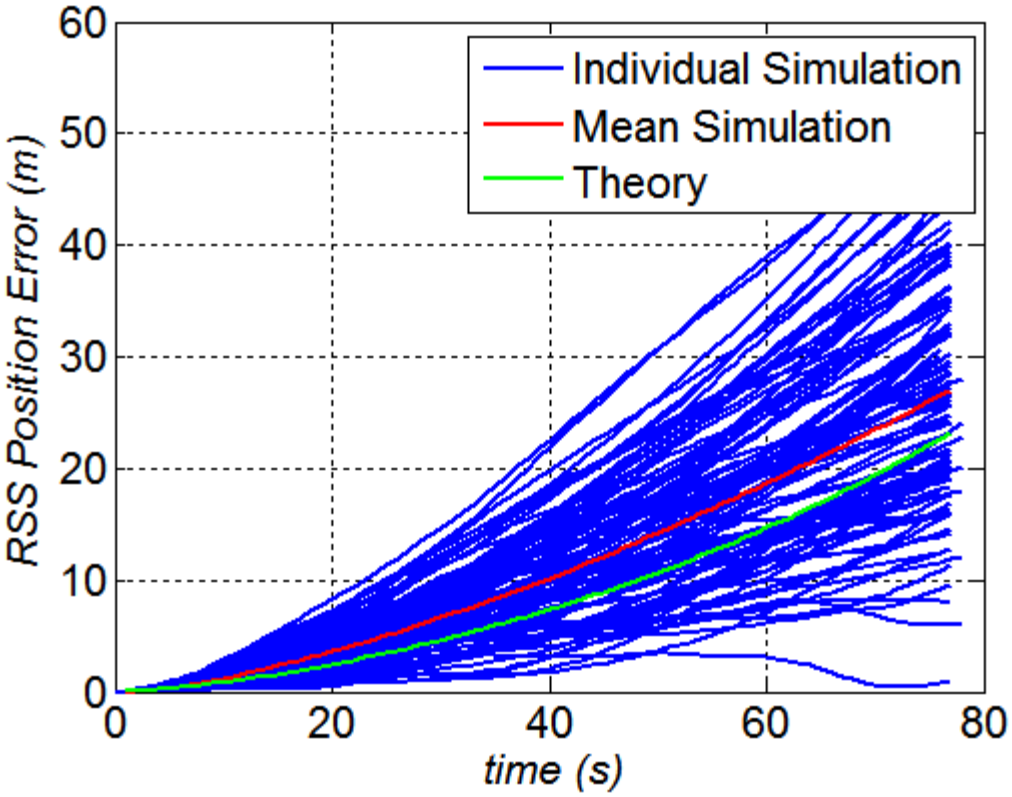

Figure 3. RSS position error due to random sensor errors.

While the position errors due to noise are acceptable, the position errors due to the remaining nuisance parameters are not. Another batch of 100 runs applying the full error budget in table 1 resulted in an estimated CEP of 15,535 m at impact, as shown in figure 4.

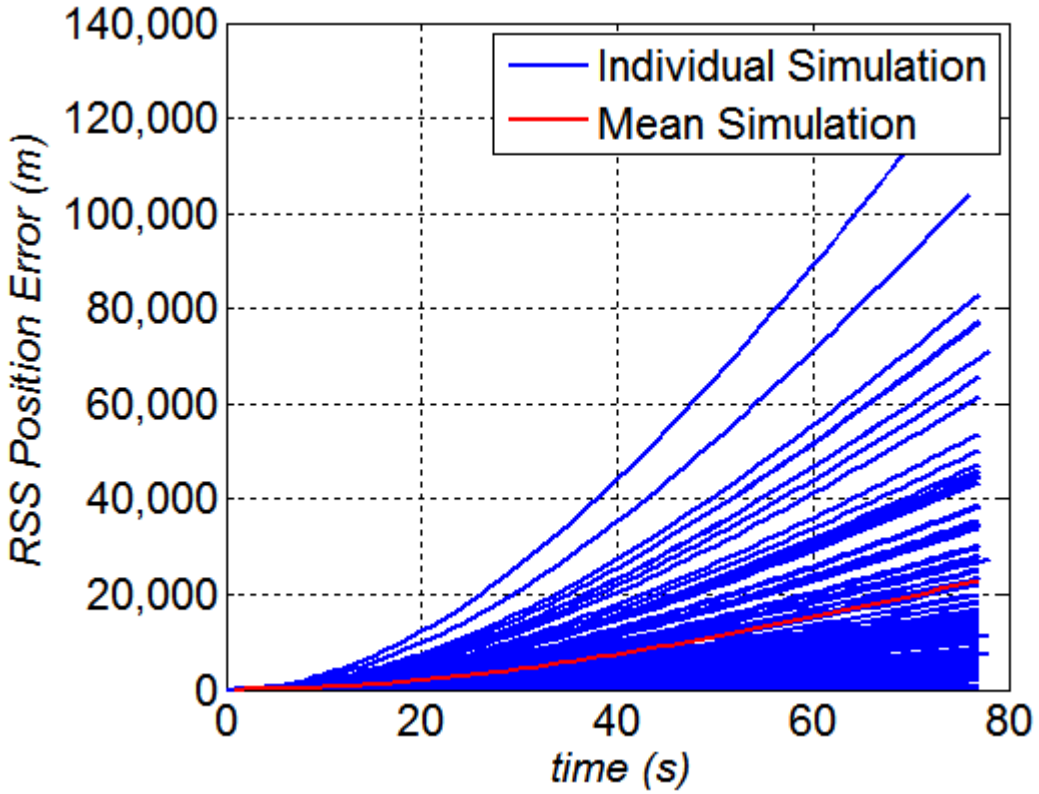

Figure 4. RSS position error due to nuisance parameters.

Now that the simulation is validated and the need for nuisance parameter estimation is clearly demonstrated, the performance of the nuisance parameter estimation algorithm is examined. A typical output for a radial accelerometer (the J axis in this case) is shown in figure 5. The raw accelerometer output is being simulated with the exact error model from equation 3 alongside the nuisance parameter state estimates. The data shows that the offset of the accelerometer is adequately represented by a bias and centripetal acceleration term. The convergence of these terms is dependent on filter tuning, as well as the magnitude of scale-factor errors, which were not accounted for in the estimator design.

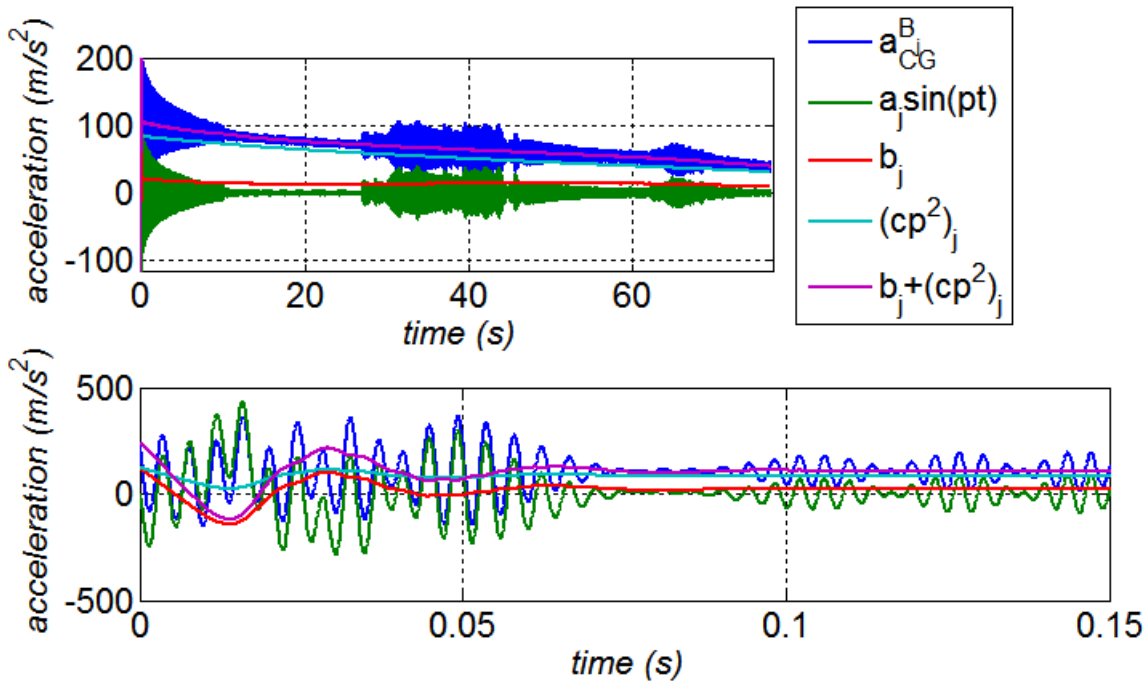

Figure 5. Typical radial accelerometer nuisance parameters.

Figure 6 demonstrates the effectiveness of the nuisance parameter estimation in correcting a typical axial accelerometer signal. The top part of the figure displays the raw output of the sensor, as well as the output after the nuisance parameters have been estimated and compensated for. Over the course of the trajectory, the compensated accelerometer almost perfectly matches the error-free accelerometer signal. The lower half of the figure displays the estimates for b_i and c_i, which are approximately constant as expected.

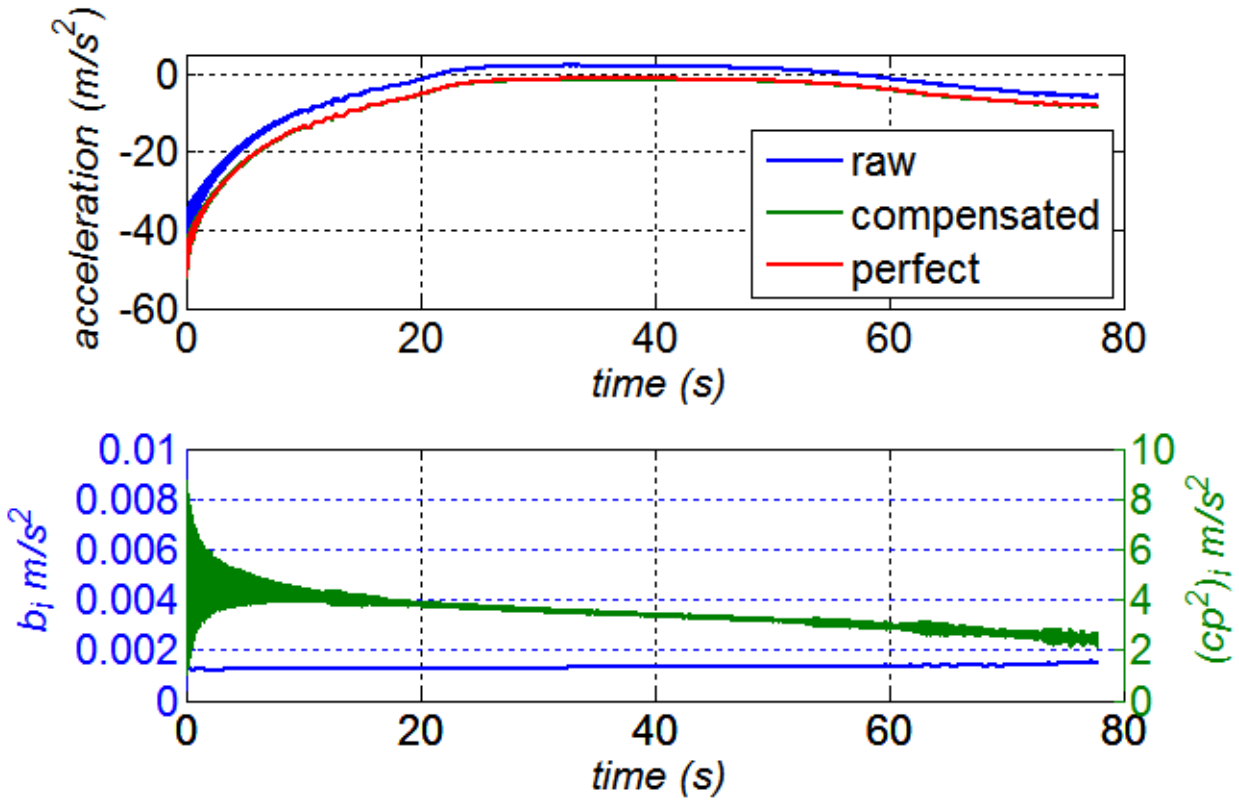

Figure 6. Typical axial accelerations and nuisance parameters.

A Monte Carlo of 100 runs was performed. The resulting CEP for the navigation algorithm was 81 m, and the RSS error trajectories are shown in figure 7. As expected, adding the nuisance parameter estimation dramatically reduces the navigation error when sensor errors are present, although the error limit due to noise alone is not reached. For reference, the impact CEP for the ballistic flight of notional artillery munitions is over 200 m at these conditions. These results illustrate that with perfect attitude information, mass properties, aerodynamics, atmosphere, and initialization, the inertial navigation with nuisance parameter estimation for guided spin-stabilized projectiles provides a navigation solution that is still an improvement over ballistic dispersion in a GPS-denied environment.

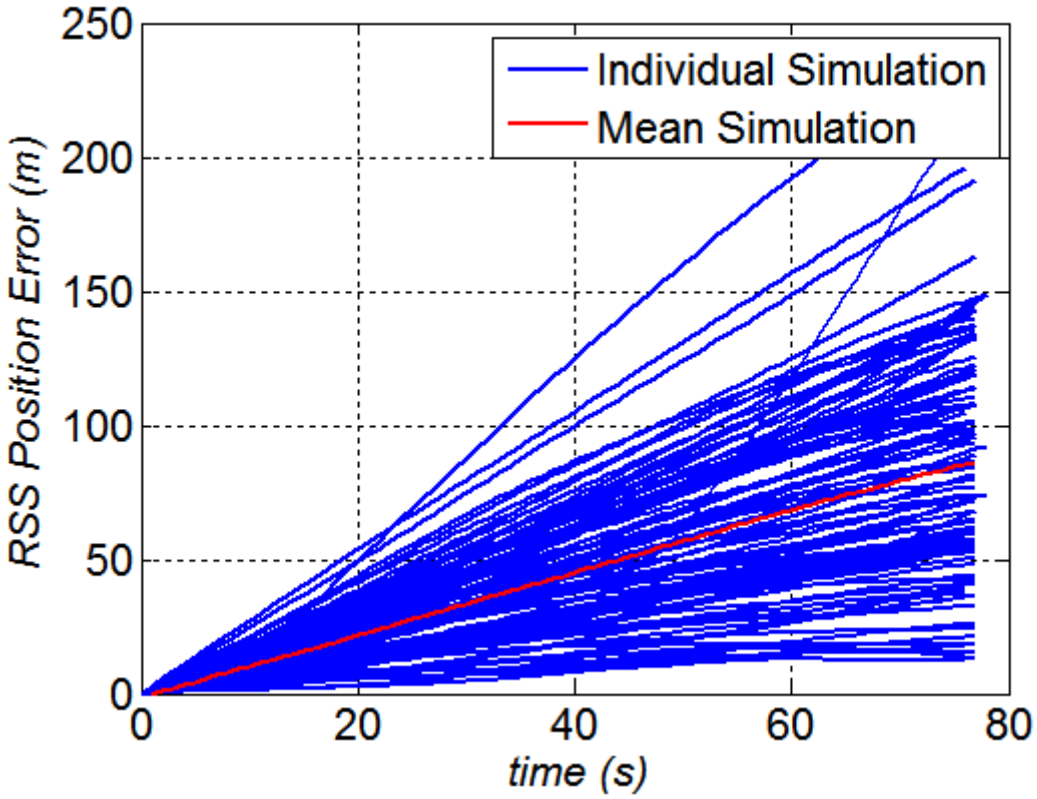

Figure 7. Monte-Carlo results with nuisance parameter estimation.

6. Conclusion

Improving gun-launched munition performance is an active research area in order to reduce munition cost, improve precision in all environments, and reduce collateral damage. Low-cost accelerometer nuisance parameter estimation for spin-stabilized projectile navigation was conducted, resulting in a mean position error of 81 m over an 80-s flight. This method is tolerant to accelerometer errors due to the novel manner in which in-flight calibration is performed. Algorithms were developed to synthesize expected launch and flight characteristics with microelectromechanical sensor modeling. Key heuristic parameters were proposed using in-flight measurement models to compensate for low-cost sensors in the spin-stabilized projectile environment. Low-cost measurements required for navigation are critical to affordably guiding a projectile to a target. This effort demonstrates that accelerometer errors in certain conditions may be reduced to a level sufficient to improve weapon accuracy in GPS-denied environments. These results do not address the error sources present in an inertial navigation solution not related to accelerometers such as initialization or attitude errors.

7. References

1. Grubb, N. D.; Belcher, M. W. Excalibur: New Precision Engagement Asset in the Warfight. *Fires* **2008**, October–December, *14–15*.

2. Wells, L. L. The Projectile GRAM SAASM for ERGM and Excalibur. Presented at IEEE/ION Position, Location, and Navigation Symposium, San Diego, CA, 13–16 March 2000.

3. Grace, J. GPS Guidance System Increases Projectile Accuracy. *IEEE Aerospace and Electronic Systems Magazine* **2000**, *15* (6), 15–17.

4. Fresconi, F. E. Guidance and Control of a Projectile With Reduced Sensor and Actuator Requirements. *Journal of Guidance, Control, and Dynamics* **2011**, *34* (6), 1757–1766.

5. Fresconi, F.; Brown, T.; Celmins, I.; DeSpirito, J.; Ilg, M.; Maley, J.; Magnotti, P.; Scanlan, A.; Stout, C.; Vazquez, E. *Very Affordable Precision Projectile Technology Development and Flight Demonstrations*; ARL-TR-5460; U.S. Army Research Laboratory: Aberdeen Proving Ground, MD, 2011.

6. Moorhead, J. S. Precision Guidance Kits (PGKs): Improving the Accuracy of Conventional Cannon Rounds. *Field Artillery* **2007**, *12*, 31–33.

7. Morrison, P. H.; Ambernston, D. S. Guidance and Control of Cannon-Launched Guided Projectile. *Journal of Spacecraft and Rockets* **1977**, *14* (6), 328–334.

8. Oskay, V.; Mermagen, W. H.; Bradley, J. W. Instrumented Drop Tests of a Slowly Rolling Parachute Payload. *Journal of Guidance and Control* **1981**, *4* (3), 267–272.

9. Regan, F. J.; Smith, J. Aeroballistics of a Terminally Corrected Spinning Projectile. *Journal of Spacecraft and Rockets* **1975**, *12* (12), 733–738.

10. McMichael, J.; Lovas, A.; Plostins, P.; Sahu, J.; Brown, G.; Glezer, A. Microadaptive Flow Control Applied to a Spinning Projectile. Presented at AIAA Atmospheric Flight Mechanics Conference, Providence, RI, 16–19 August 2004.

11. Fresconi, F.; Cooper, G. R.; Celmins, I.; DeSpirito, J.; Costello, M. Flight Mechanics of a Novel Guided Spin-Stabilized Projectile Concept. *Journal of Aerospace Engineering* **2011**, *226*, 327–340.

12. Theodoulis, S.; Gassmann, V.; Wernert, P.; Dritsas, L.; Kitsios, I.; Tzes, A. Guidance and Control Design for a Class of Spin-Stabilized Fin-Controlled Projectiles. *Journal of Guidance, Control, and Dynamics* **2013**, *36*, 517–531.

13. Mermagen, W. H. High-G Resistant Electronic Fuse of Projectile Payloads. *Journal of Spacecraft and Rockets* **1971**, *8* (8), 900–903.

14. Brown, T.; Davis, B.; Hepner, D.; Faust, J.; Myers, C.; Muller, P.; Harkins, T.; Hollis, M.; Miller, C.; Placzankis, B. Strap-Down Microelectromechanical Sensors for High-G Munition Applications. *IEEE Transactions on Magnetics* **2001**, *37* (1), 336–342.

15. Carlucci, D. E., Frydman, A. M.; Cordes J. A. Mathematical Description of Projectile Shot Exit Dynamics (Set-Forward). *Journal of Applied Mechanics* **2013**, *80*, 031501-1–9.

16. Habibi, S.; Cooper, S. J.; Stauffer, J. M. Gun Hard Inertial Measurement Unit Based on MEMS Capacitive Accelerometer and Rate Sensor. Presented at AIAA Atmospheric Flight Mechanics Conference, Providence, RI, 16–19 August 2004.

17. Sheard, K.; Scaysbrook, I.; Cox, D. MEMS Sensor and Integrated Navigation Technology for Precision Guidance. Presented at IEEE/ION Position, Location, and Navigation Symposium, Monterey, CA, 5–8 May 2008.

18. Rogers, J.; Costello, M. A Low-Cost Orientation Estimator for Smart Projectiles Using Magnetometers and Thermopiles. *Navigation* **2012**, *59* (1), 9–24.

19. Rogers, J.; Costello, M.; Harkins, T. Hamaoui, M. Effective Use of Magnetometer Feedback for Smart Projectile Applications *Navigation* **2011**, *58* (3), 203–219.

20. Maley, J. Roll Orientation from Commercial Off-The-Shelf (COTS) Sensors in the Presence of Inductive Actuators. Presented at Institute of Navigation Joint Navigation Conference, Colorado Springs, CO, 27–30 June 2011.

21. Erickson, M.; Costello, M. Production Line Calibration for Sensors on Actively Controlled Bullets. *Journal of Manufacturing Science and Engineering* **2004,** *126*, 368–376.

22. Murphy, C. Free Flight of Symmetric Missiles; U.S. Army Ballistics Research Laboratory: Aberdeen Proving Ground, MD, 1963.

23. Nicolaides, J. *On Missile Flight Dynamics*; Catholic University of America: Washington D.C., 1963.

24. Cooper, G.; Fresconi, F; Costello, M. Flight Stability of Asymmetric Projectiles With Activating Canards. *Journal of Spacecraft and Rockets* **2012**, *49* (1), 130–135.

25. Fresconi, F.; Harkins, T. Experimental Flight Characterization of Asymmetric and Manuevering Projectiles from Elevated Gun Firings. *Journal of Spacecraft and Rockets* **2012**, *49*, 1120–1130.

26. Fresconi, F.; Cooper, G.; Costello, M. Practical Assessment of Real-Time Impact Point Estimators for Smart Weapons. *Journal of Aerospace Engineering* **2011**, *24* (1), 1–11.

27. Koifman, M.; Bar-Itzhack, I. Inertial Navigation System Aided by Aircraft Dynamics. *IEEE Transactions on Control Systems Technology* **1999**, *7* (4), 487–493.

28. Fairfax, L. D.; Fresconi, F. E. Position Estimation for Projectiles Using Low-Cost Sensors and Flight Dynamics. *Journal of Aerospace Engineering* **2013;** accepted for publication.

29. Greenwood, D. T. *Principles of Dynamics*; Prentice-Hall: Englewood Cliffs, NJ, 1965.

30. Simon, D. *Optimal State Estimation: Kalman, H-infinity, and Nonlinear Approaches*; Wiley-Interscience: Hoboken, NJ, 2008.

31. Crassidis, J. L.; Junkins,J. L. *Optimal Estimation of Dynamic Systems*; Chapman & Hall/CRC: Boca Raton, LA, 2004.

List of Symbols, Abbreviations, and Acronyms

Nomenclature

$\vec{a}_M^B$	Specific force at measurement location in body fixed coordinates measured by accelerometer
m	Projectile mass
$\vec{F}_A$	Aerodynamic forces
$\vec{\dot{\omega}}_{B/I}$	Angular acceleration of body with respect to inertial coordinates
$\vec{r}_{CG\to M}$	Moment arm from accelerometer location to projectile center of gravity
$\vec{a}_{CG}^B$	Specific force at center of gravity in body fixed coordinates measured by accelerometer
$\vec{S}_M$	Scale factor in accelerometer measurement
$\vec{T}_{MB}$	Transformation from the accelerometer measurement coordinates to the body fixed coordinates
$\vec{\varepsilon}_{r_{CG\to M}}$	Accelerometer misplacement error
$\vec{\varepsilon}_B$	Accelerometer bias error
$\vec{\varepsilon}_N$	Accelerometer white noise error
$\vec{e}_{\vec{a}_{CG}^B}$	Error in accelerometer measurement at center of gravity
c_i, c_j, c_k	Accelerometer roll-dependent nuisance parameter
b_i, b_j, b_k	Accelerometer bias nuisance parameter
$p, \dot{p}$	Roll rate, roll acceleration
a_i, a_j, a_k	Accelerometer amplitude heuristic nuisance parameters
ρ	Air density
V	Total projectile velocity with respect to surrounding air
D	Projectile diameter

C_X	Axial force coefficient
C_{l_p}	Roll-damping moment coefficient
$\vec{Y}$	Measurement
$\vec{Y}^*$	Predicted measurement
$\vec{X}, \dot{\vec{X}}$	State vector, state vector derivative
$\vec{A}$	State transition matrix in continuous time
$\vec{F}$	State transition matrix in discrete time
$t, \Delta t$	Time, time step
$\vec{H}$	Measurement matrix
$\vec{P}$	Covariance matrix
$\vec{Q}$	Process model covariance matrix
$\vec{K}$	Kalman gain
$\vec{R}$	Measurement covariance matrix
$\vec{I}$	Identity matrix
$\hat{a}_{CG}^{B}$	Compensated specific force at center of gravity in body fixed coordinates
$\vec{a}_{CG}^{I}$	Acceleration at the center of gravity in inertial coordinates
$\vec{T}_{BI}$	Transformation matrix from body fixed coordinates to inertial coordinates
$\vec{g}$	Gravity vector in inertial coordinates
$\sigma_{err}(t)$	Position standard deviation
σ_{drift}	Accelerometer bias drift standard deviation
σ_{noise}	Accelerometer white noise standard deviation

NO. OF COPIES	ORGANIZATION
1 (PDF)	DEFENSE TECHNICAL INFORMATION CTR DTIC OCA
1 (PDF)	DIRECTOR US ARMY RESEARCH LAB IMAL HRA
1 (PDF)	DIRECTOR US ARMY RESEARCH LAB RDRL CIO LL
1 (PDF)	GOVT PRINTG OFC A MALHOTRA
1 (PDF)	DIR USARL RDRL WML E L FAIRFAX

INTENTIONALLY LEFT BLANK.